JOURNAL OF GEOPHYSICAL RESEARCH, VOL. 101, NO. D3, PAGES 6899-6909, MARCH 20, 1996

# Atmospheric sulfur cycling in the tropical Pacific marine boundary layer (12°S, 135°W): A comparison of field data and model results 1. Dimethylsulfide

S. A. Yvon,[1,4] E. S. Saltzman,[1] and D. J. Cooper,[1,5] T. S. Bates,[2] and A. M. Thompson[3]

**Abstract.** Shipboard measurements of atmospheric and seawater DMS were made at 12°S, 135°W for 6 days during March 1992. The mean seawater DMS concentration during this period was 4.1 ± 0.45 nM (1σ, $n$ = 260) and the mean atmospheric DMS mole fraction was 453 ± 93 pmol mol$^{-1}$ (1σ, $n$ = 843). Consistent atmospheric diel cycles were observed, with a nighttime maximum and daytime minimum and an amplitude of approximately 85 pmol mol$^{-1}$. Photochemical box model calculations were made to test the sensitivity of atmospheric DMS concentrations to the following parameters: 1) sea-to-air flux, 2) boundary layer height, 3) oxidation rate, and 4) vertical entrainment velocities. The observed relationship between the mean oceanic and atmospheric DMS levels require the use of an air-sea exchange coefficient which is at the upper limit end of the range of commonly used parameterizations. The amplitude of the diel cycle in atmospheric DMS is significantly larger than that predicted by a photochemical model. This suggests that the sea-to-air DMS flux is higher than was previously thought, and the rate of daytime oxidation of DMS is substantially underestimated by current photochemical models of DMS oxidation.

## Introduction

Dimethylsulfide is the principle gaseous precursor for sulfate aerosol over the oceans, and it has been suggested that various feedback loops may link DMS emissions and global climate [*Nguyen et al.*, 1983, *Shaw*, 1983; *Charlson et al.*, 1987; *Bates et al*, 1987, *Legrand et al.*, 1988, 1991] DMS is ultimately derived from the activity of phytoplankton in seawater and is ubiquitous in the surface oceans and marine atmosphere. In clean marine air, DMS is oxidized primarily through reaction with the hydroxyl (OH) radical and has a lifetime of the order of a few days DMS exhibits diel cycles of considerable amplitude because of its relatively short lifetime and photochemical sink. These diel cycles have been observed by several investigators [*Maroulis and Bandy*, 1977; *Andreae and Raemdonck*, 1983, *Andreae et al.*, 1985; *Saltzman and Cooper*, 1988; *Cooper and Saltzman*, 1993] and have been shown to be generally consistent with gas transfer velocity and photochemical models [*Logan et al.*, 1981, *Thompson and Lenschow*, 1984; *Thompson and Cicerone*, 1982; *Graedel*, 1979; *Chatfield and Crutzen*, 1984; *Toon et al.*, 1987; *Thompson et al.*, 1990]. Under favorable conditions (uniform sea surface DMS concentrations, well-characterized meteorology, clean air mass chemistry) the diel variability in DMS can provide quantitative verification of parameterizations of its air-sea fluxes and atmospheric reactivity. In this study we present measurements of the diel variability in DMS in the equatorial Pacific tropical trade wind regime where conditions should be favorable for the interpretation of such data. Measurements of seawater and atmospheric DMS were made during an International Global Atmospheric Chemistry/Marine Aerosols and Gases Experiment (IGAC/MAGE) cruise aboard the R/V *John V. Vickers* in the tropical South Pacific Ocean in February and March of 1992. The data presented here were obtained at a station at 12°S, 135°W which was occupied from March 3 to 10, 1992.

## Experimental Methods

### Atmospheric DMS (Rosenstiel School of Marine and Atmospheric Science)

The atmospheric DMS data reported here were collected by using a technique described in detail by *Cooper and Saltzman* [1993]. The sample inlet was mounted on the front of a laboratory van, which was bolted to the deck on the flying bridge. The van was located forward of the ship's stacks, and the inlet was approximately 15 m above sea level. The sample airstream was drawn at 1 standard liter per minute through a cold (0°C) neutral potassium iodide bubbler to remove oxidants. The oxidant free air was drawn first through a Teflon tube at -20°C containing Teflon wool to remove water and then through another tube containing Tenax at -20°C to trap DMS. Both tubes were contained in a block of aluminum which was heated and cooled with a thermoelectric module and a temperature controller. This preconcentration step took approximately 10 min, depending upon the concentrations being measured. The current was then reversed on the thermoelectric module, and the aluminum block was heated to 80°C, allowing the Tenax to heat up and release the DMS, which was then transferred onto a second cold Tenax focusing trap. This second trap was then heated, and the sample was injected onto a Chromosil 330 packed column. The DMS was chromatographically separated isothermally at 50°C with DMS eluting at approximately 6 min

[1] Rosenstiel School of Marine and Atmospheric Science, University of Miami, Miami, Florida
[2] NOAA Pacific Marine and Environmental Laboratory, Seattle, Washington.
[3] NASA Goddard Space Flight Center, Greenbelt, Maryland.
[4] Now at NOAA Climate Monitoring and Diagnostics Laboratory, Boulder, Colorado.
[5] Now at Plymouth Marine Laboratory, Plymouth, England.



Paper number 95JD03356
0148-0227/96/95JD-03356 $05.00

and detected by a flame photometric detector. The lower limit of detection was 3 pmol $mol^{-1}$.

The instrument was calibrated with aqueous standards [*Saltzman and Cooper*, 1988]. A glass tee containing silanized glass wool was fitted with a septum. The standard was injected onto the glass wool, and a stream of zero air was passed through the tee, where the DMS was entrained and analyzed as described above. The aqueous standard was prepared through a two-step volumetric dilution of pure DMS resulting in 1.0 μM DMS in water.

### Seawater and Atmospheric DMS (Pacific Marine and Environmental Laboratory)

The seawater DMS measurements reported here were made by investigators from the National Oceanographic and Atmospheric Administration's Pacific Marine and Environmental Laboratory (NOAA/PMEL). The seawater samples were immediately analyzed aboard ship for DMS concentrations by using an automated collection/purge and trap system. Samples were collected from the ship's seawater pumping system at a depth of approximately 5 m. The seawater line ran to the analytical system, where 2-10 mL of sample were valved into a Teflon gas stripper. The samples were purged with hydrogen at 60 mL/min for 5-20 min. Air samples were pulled through a KI bubbler to eliminate oxidant interferences [*Cooper and Saltzman*, 1993]. Water vapor in either the air or the purged seawater sample stream was removed by passing the air through a -30°C Teflon tube filled with glass wool. DMS was then trapped in a -30°C Teflon tube filled with Tenax. At the end of the sampling/purge period the coolant was pushed away from the trap, and the trap was electrically heated. DMS was desorbed onto a DB-1 megabore fused silica column, where the sulfur compounds were separated isothermally at 40°C and quantified with a flame photometric detector. The detector was modified as described by *Bates et al.* [1990]. The detection limit during MAGE 92 was approximately 0.8 pmol. The system was calibrated by using gravimetrically calibrated permeation tubes. The precision of the analysis, based on both replicate analyses of a single water sample and replicate analyses of a standard introduced at the inlet of the air sample line, was typically ±8%. The performance of the system was monitored regularly by running blanks and standards through the entire system. Values reported here have been corrected for recovery losses. System blanks were below detection limit. During the cruise the PMEL system was intercalibrated with the Rosenstiel School of Marine and Atmospheric Science (RSMAS) system and agreed to within 4%.

## Meteorology

Ten-day air mass back trajectories on the 1000-hPa level were calculated from the National Meteorological Center's wind analyses for the Pacific region (R. Artz, NOAA Atmospheric Research Laboratory). An example of a typical air mass back trajectory for the 6 days of time series measurements was plotted on satellite images (RSMAS Remote Sensing Facility) showing the sea surface temperature in the region near the ship. The air masses being sampled were over the ocean for at least 10 days before reaching the MAGE station, and the sea-surface temperature was fairly homogeneous along the trajectory of the air masses. The airflow was predominantly easterly and originated in the Southeast Pacific gyre.

Balloon radiosondes were launched just before dawn (local time), just after solar noon, and just before sunset each day while occupying the MAGE station. Radiometer data indicated that the solar noon occurred at approximately 1230 hours local time. Figure 1 shows an example of a typical radiosonde from the MAGE station. A temperature inversion can be seen at 2200 m along with a sharp decrease in relative humidity, indicating the top of the cloud-containing layer and the bottom of the trade wind inversion. This layer is highly stratified and acts as a barrier to vertical mixing with the free troposphere. Also, note that there is a drop in the relative humidity and a small change in the temperature and potential temperature gradients at approximately 600 m, signaling the top of the mixed layer.

Traditionally, the marine boundary layer is thought to extend to the top of the cloud-containing layer. However, there is uncertainty about the extent to which the bottom of the cloud-containing layer acts as a barrier to vertical mixing. The turnover rate in the mixed layer is of the order of 10-20 min [*Stull*, 1988]. This is much less than the lifetime of trace gases such as DMS. Therefore the mixed layer should be well mixed with respect to DMS. However, mixing into the cloud-containing layer occurs sporadically and is enhanced during periods of active convection through cumulus clouds.

A camera with a wide angle lens (180°) was used to photograph the sky during daylight hours throughout the cruise. This was done to allow us to assess the cloud cover conditions for use in the photochemical model. During the 6 days of the MAGE station (12°S, 135°W) the weather conditions were generally sunny and mostly clear. A few clouds and rain showers passed over the ship during this period.

## Results and Discussion

### Seawater DMS

The results of the seawater DMS measurements from the MAGE station are shown in Figure 2a. A slight increasing trend

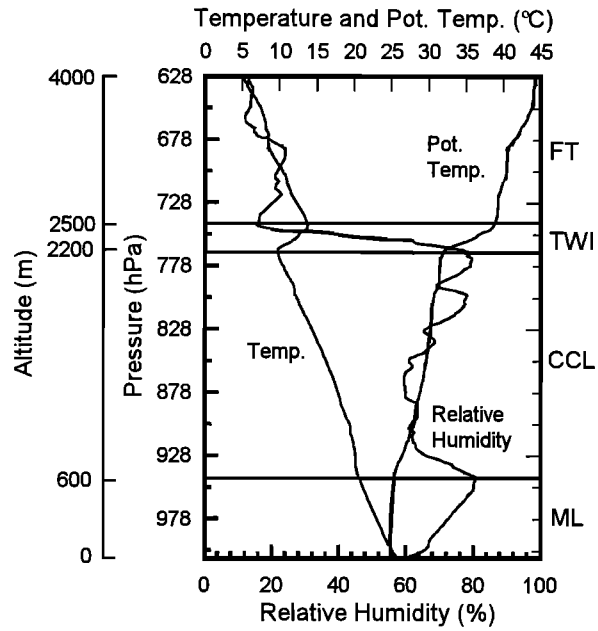


**Figure 1.** A typical radiosonde from the MAGE station from J.D. 66 at 1400 GMT. The horizontal lines indicate the boundaries between the different atmospheric layers: mixed layer (ML), cloud-containing layer (CCL), trade wind inversion (TWI), and free troposphere (FT). The temperature and potential temperature curves are plotted along the top *x* axis, and the relative humidity curve is plotted along the bottom *x* axis.

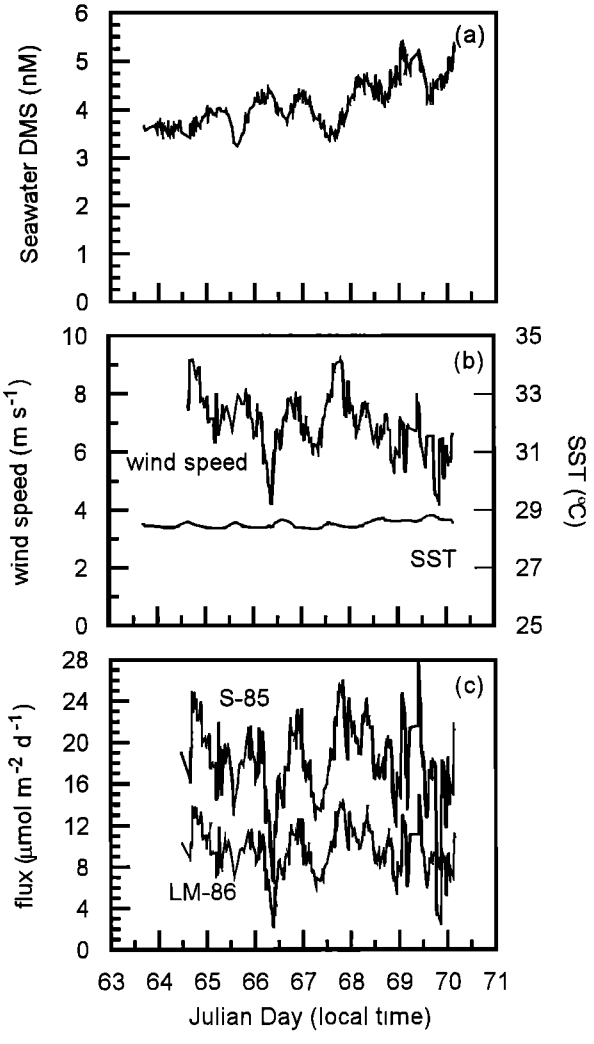


**Figure 2.** (a) The seawater DMS data collected at 12°S, 135°W plotted as a time series, (b) wind speed and sea surface temperature (SST) plotted as a time series, and (c) the calculated sea-to-air flux of DMS using the *Liss and Merlivat* [1986[ (LM-86) and the *Smethie et al.* [1985] (S-85) relationships between gas exchange and wind speed.

can be seen in the data beginning at day 67.5 and continues to the end of the MAGE station. However, the overall range of concentrations is small, and seawater DMS averages 4.1 ± 0.45 nM (1σ, $n$ = 260) for the duration of the station. These seawater DMS levels are among the highest levels reported for this region. The global mean seawater DMS concentration for tropical oligotrophic waters is 2.4 nM [*Andreae*, 1990]. Surface seawater DMS concentrations in the tropical South Pacific at the same time of year in 1990 were approximately 2.9 nM at 10°S, 145°W [*Bates et al.*, 1993].

The MAGE station was located inside the South Pacific gyre and should be representative of remote oligotrophic waters, because nutrient and chlorophyll concentrations were low and biological DMS turnover rates were low [*Kieber et al.*, 1996]. The nutrient (nitrate) levels found in the surface seawater were below the detection limit (<0.05 µM) for the most of the time series. One exception occurred near the beginning of day 67 where surface seawater nitrate concentrations rose to detectable levels and then dropped off to below the detection limit within a 12-hour period. The chlorophyll concentrations were uniformly low (0.1 µg $L^{-1}$) during the course of the time series and did not reflect the increase in nitrate levels observed on day 67. Seawater DMS concentrations are usually controlled by the biological turnover rate [*Kiene and Bates*, 1990]; however, during this study, biological consumption, air-sea exchange and photolysis contributed almost equally to DMS removal in the surface mixed layer [*Kieber et al.*, 1996].

The sea surface DMS concentration (Figure 2a) shows evidence of a diel cycle with a nighttime maximum and a daytime minimum. This suggests a photochemical pathway for the removal of DMS in the water column [*Brimblecombe and Shooter*, 1986]. In order to examine the average diel cycle in seawater DMS for the MAGE station the data were sorted according to the time of day at which the sample was taken. The results from averaging the data using 2-hour bins are shown in Figure 3. The amplitude of the diel cycle in seawater DMS is approximately 0.2 nM, which is about 5% of the mean concentration. Thus this variation does not introduce a significant diel variability in the sea-to-air flux estimates as discussed below.

The sea surface temperatures and wind speeds recorded while at the MAGE station are shown in Figure 2b. The sea-surface temperatures averaged 28.5 ± 0.12°C (1σ, $n$ = 260), and the wind speeds range from 4.2 to 9.2 m $s^{-1}$ with a mean wind speed of 7.11 ± 1.12 m $s^{-1}$ (1σ, $n$ = 260). This is greater than the 3 m $s^{-1}$ threshold for production of capillary waves, however, it is less than the 13.6 m $s^{-1}$ necessary for generation of breaking waves where bubble entrainment may enhance gas transfer [*Liss and Merlivat*, 1986; *Upstill-Goddard et al.*, 1990].

The magnitude of the oceanic source of DMS at the MAGE station can be estimated from the observed sea surface concentrations, wind field, and temperature. We use the general expression $\text{Flux}=K\Delta C=K(C_gH-C_l)$ [*Liss and Slater*, 1974], where $K$ is a gas transfer velocity or gas exchange coefficient and $H$ is the dimensionless Henry's law constant [*Dacey et al.*, 1984]. For DMS the gas transfer velocity is determined by the properties of the liquid phase. It has been shown in wave tank and lake experiments that gas exchange varies with $(Sc)^{-n}$, where $n$=1/2 for the wind regime encountered in this study (4-10 m $s^{-1}$) [*Liss and Merlivat*, 1986; *Jähne et al.*, 1987; *Watson et*

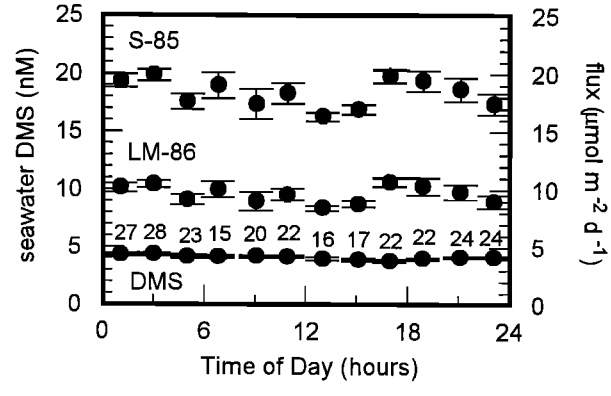


**Figure 3.** Results from measurements of seawater DMS and the sea-to-air flux of DMS using the LM-86 and S-85 relationships averaged using 2-hour bins. The error bars shown are for one standard error ($\sigma/(n^{1/2})$) in the mean, where $n$ for each 2-hour bin is given above its respective DMS point. The value for $n$ is the same for each of the corresponding bins for LM-86 and S-85.

*al.*, 1991]. Various relationships between gas transfer velocity and wind speed have been derived from wave tank, in situ tracer studies in lakes, and natural and bomb-derived $^{14}C$. The most commonly cited relationship is that of *Liss and Merlivat* [1986]. For the wind speeds encountered during this study the *Liss and Merlivat* [1986] relationship (hereafter referred to as LM-86) is given as

$$K_{CO_2}(600) = 2.85U - 9.65 \qquad 3.6 \text{ m s}^{-1} < U < 13 \text{ m s}^{-1} \quad (1)$$

where U is wind speed (m $s^{-1}$) and 600 is the Schmidt number for $CO_2$ at 20°C. This relationship is supported by various wave tank studies [*Holmen and Liss*, 1984; *Jähne et al.*, 1987]. *Smethie et al.* [1985; hereafter referred to as S-85] proposed the following linear relationship based on $^{222}Rn$ deficit measurements in the North Atlantic:

$$K_{Rn}(885) = 1.1(U - 3) \quad (2)$$

where $U$ is the wind speed (m $s^{-1}$) and 885 is the Schmidt number for Rn at 20°C. The gas transfer velocity obtained in this way is approximately a factor of 2 larger than that calculated from LM-86 at the global mean wind speed of 7.4 m $s^{-1}$. The difference between these relationships reflects the uncertainty in our current understanding of the process of air-sea gas exchange. We have calculated the DMS flux using both relationships, using the temperature dependent Schmidt number of DMS from *Saltzman et al.* [1993]. A gas transfer velocity and sea-to-air flux of DMS is calculated for each seawater DMS sample measured during the MAGE station (Figure 2c). The mean DMS flux for the MAGE station is 9.65 ± 2.49 μmol $m^{-2}$ $d^{-1}$ (1σ, $n$ =260), using LM-86, and 18.43 ± 3.97 μmol $m^{-2}$ $d^{-1}$ (1σ , $n$ =260), using S-85 (Table 1). Binning these data into 2-hour averages does not reveal a diel cycle in the sea-to-air flux (Figure 3). Both fluxes are much higher than the global mean DMS flux of 5 μmol $m^{-2}$ $d^{-1}$ [*Bates et al*, 1992] for tropical oligotrophic waters. *Bates et al.* [1993] also calculated a sea-to-air DMS flux for this region from field measurements made during the SAGA 3 experiment. Their calculated DMS flux is 12 μmol $m^{-2}$ $day^{-1}$, which is also higher than the global average for this region.

## Atmospheric DMS

The results of the atmospheric DMS measurements made by the RSMAS instrument during the MAGE station are shown in Figure 4. As mentioned earlier, the results of atmospheric DMS measurements made with the NOAA/PMEL instrument agreed with those from the RSMAS instrument to within ±4%. The mean concentration for the MAGE station is 453 ± 93 pmol $mol^{-1}$ (1σ, $n$ = 843). These are among the highest levels of atmospheric DMS observed in the remote marine boundary layer [*Andreae*, 1990; *Quinn et al.*, 1990; *Bates et al.*, 1992]. However, high atmospheric DMS concentrations are consistent with the results from measurements made in this region in the past [*Huebert et al.*, 1993]. There do not appear to be any long-term (>1 day) trends in the data. However, a pronounced diel cycle with an amplitude (defined here as the difference between the mean and the extreme) of 85 pmol $mol^{-1}$ can be seen in the data with a maximum just before dawn and a late afternoon minimum (Figure 4b). Qualitatively, this cycle appears to be consistent with current photochemical models of DMS oxidation in a well-mixed marine boundary layer where reaction with the hydroxyl (OH) radical is the primary sink.

**Table 1.** Average Seawater Data for the MAGE Station With Average Calculated Gas Transfer Velocities and Fluxes

| Parameter | Station Average | Standard Deviation |
|---|---|---|
| Seawater DMS concentration, nM | 4.13 | 0.47 |
| SST, °C | 28.5 | 0.12 |
| Wind speed, m $s^{-1}$ | 7.11 | 1 12 |
| LM-86 piston velocity, m $d^{-1}$ | 2.49 | 0.75 |
| LM-86 flux, μmol $m^{-2}$ $d^{-1}$ | 9.65 | 2.49 |
| S-85 piston velocity, m $d^{-1}$ | 4.74 | 1.20 |
| S-85 flux, μmol $m^{-2}$ $d^{-1}$ | 18.43 | 3.97 |

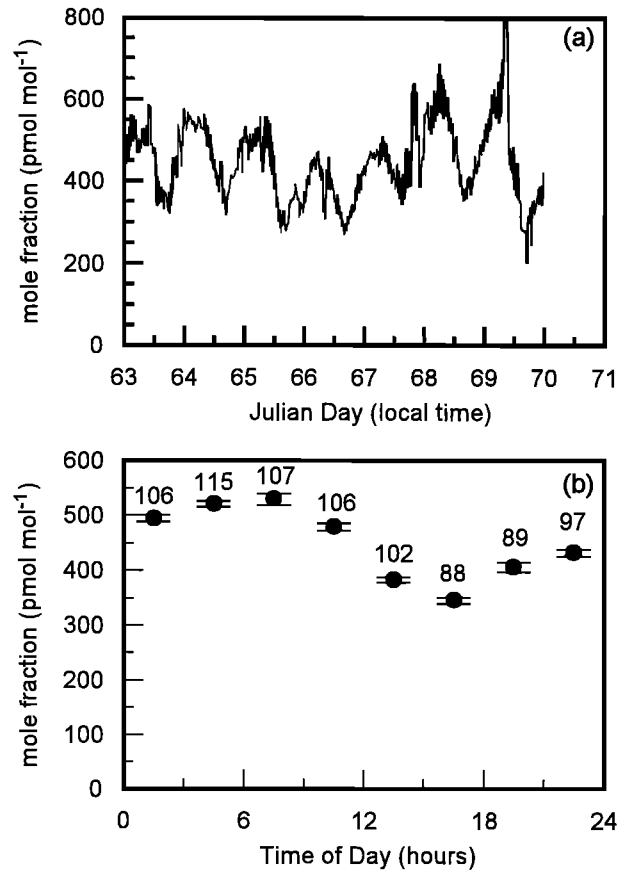


**Figure 4.** Atmospheric DMS data for MAGE station 12°S, 135°W (a) plotted as a time series, and (b) averaged over 3-hour intervals for the entire MAGE station. The error bars indicate one standard error ($\sigma/(n^{1/2})$) about the mean, where n is given above each averaged point. The averaged data have been adjusted so that 12 is the solar noon.

## Modeling

A time-dependent photochemical box model is used in an attempt to quantitatively model the field data. A detailed description of this model is given by *Yvon and Saltzman* [1993]. Two modifications were made to the model for use in this study: (1) the inclusion of a vertical entrainment velocity for the incorporation of free tropospheric air in the boundary layer and (2) the kinetic distribution of total $NO_x$ among the various reservoir species (NO, $NO_2$, $NO_3$, $N_2O_5$). The approach used here is to model the marine boundary layer as a well-mixed box.

The results from measurements of other photochemically important species are used to establish temporal profiles of important oxidants. A constant source flux of DMS is imposed, and the model is run until the resulting diel DMS profile is constant from one day to the next.

**Model description.** The reactions included in the model are shown in Table 2 with their rate constants. The rate constants for these reactions are taken from *NASA Panel for Data Evaluation* [1990; hereinafter *NASA Evaluation 9*], *Russell et. al.* [1986], *Johnston et. al.* [1986], *Thompson and Lenschow* [1984], and *IUPAC Subcommittee on Gas Kinetic Data Evaluation for Atmospheric Chemistry* [1992; hereinafter *IUPAC Supplement IV*] A variable time step fourth-order Runge-Kutta routine [*Press et al.*, 1986] is used to solve the rate expressions generated by these reactions. The rate expression for DMS is shown below:

$$\frac{d[\mathrm{DMS}]}{dt} = \frac{\mathrm{Flux}}{\mathrm{MMD}} - [\mathrm{DMS}]\left(k_{89}[\mathrm{OH}] + k_{88}[\mathrm{NO_3}]\right) - \frac{V_{ent}}{\mathrm{MMD}}[\mathrm{DMS}] \quad (3)$$

where [$X$] ($X$= DMS, OH, $NO_3$) is the concentration of $X$ (molecule $cm^{-3}$) , Flux is the sea-to-air-flux of DMS ($cm^{-2}$ $s^{-1}$), MMD is the model mixing depth (cm), $k_{88}$ and $k_{89}$ are the rate constants for reactions R88 and R89 respectively (see Table 1), and $V_{ent}$ is the vertical entrainment velocity (cm $s^{-1}$), which will be discussed in the next section. Similar equations are solved for 25 other species, while 13 short-lived species are calculated by using steady state equations. A simple constant rainout parameter is used for the heterogeneous loss of PAN, $HNO_3$, HCHO, $CH_3CHO$, $CH_3OOH$, $C_2H_5OOH$, and $H_2O_2$. The boundary conditions are defined by a fixed boundary layer height (BLH) and a constant source flux of DMS.

The photolysis rate constants for the reactions shown in Table 3 are calculated from the following equation [*Finlayson-Pitts and Pitts*, 1986]

$$jX = \sum_{i} \sigma_X(\lambda_i, T)\,\Phi_X(\lambda_i, T)\,\Omega_{total}(\lambda_i)\,\Delta\lambda \quad (4)$$

where $\sigma_X(\lambda_i,T)$ is the absorption cross section ($cm^{-2}$) for species $X$ at wavelength $\lambda$ and temperature $T$, $\Phi_X(\lambda_i,T)$ is the quantum yield for the photolysis of $X$ as a function of wavelength and temperature, and $\Omega_{total}(\lambda_i)$ is the total actinic flux (photons $cm^{-2}$ $s^{-1}$) for that wavelength interval ($i$). The actinic flux at Earth's surface is calculated from a two-stream radiative transfer algorithm based on that of *Thompson* [1984]. The absorption cross sections and quantum yields are taken from *NASA Evaluation 9* [1990], *IUPAC Supplement IV* [1992], *Molina and Molina* [1989], *Vaghjani and Ravishankara* [1989], *Wayne et al.* [1991], and *Griggs* [1968] as described by *Yvon and Saltzman* [1993].

**Input Data.** The input conditions common to all model runs are shown in Table 4. $O_3$ and CO were measured aboard ship and had mean mole fractions of 9.3 nmol $mol^{-1}$ and 60 nmol $mol^{-1}$, respectively [J. Johnson, personal communication, 1992]. These mole fractions are similar to the levels observed in this region during the SAGA 3 experiment [*Thompson et al.*, 1993; *Bates et al.*, 1993]. Methane concentrations are assumed to be similar to those previously measured in the tropical South Pacific [*Bates et al.*, 1993] with a 14 nmol $mol^{-1}$ increase per year [*Fraser et al.*, 1986; *Steele et al.*, 1992] resulting in 1.79 μmol $mol^{-1}$ $CH_4$. The mean $H_2O_2$ concentration is also assumed to be similar to the results of measurements made during the SAGA 3 experiment [*Thompson et al.*, 1993]. The nonmethane hydrocarbon ($C_2H_4$ and $C_2H_6$) concentrations are taken from the results of *Donahue and Prinn* [1993] and *Atlas et al.* [1993]. Temperature and relative humidity were monitored continuously and logged with the NOAA/PMEL data logging system. Mean values for the duration of the MAGE station are used in the model. The mixing depth for the base case model simulation is

**Table 2.** Chemical Reactions Used in the Photochemical Model and Their Rate Coefficients

| | Reaction | Rate Coefficient |
|---|---|---|
| (R1) | $O(^1D) + N_2 \rightarrow O$ | $k = 1.8 \times 10^{-11} \exp(110/T)$ |
| (R2) | $O(^1D) + O_2 \rightarrow O$ | $k = 3.2 \times 10^{-11} \exp(70/T)$ |
| (R3) | $O(^1D) + H_2O \rightarrow 2OH$ | $k = 2.2 \times 10^{-10}$ |
| (R4) | $O(^1D) + CH_4 \rightarrow OH + CH_3$ | $k = 1.4 \times 10^{-10}$ |
| (R5) | $O(^1D) + H_2 \rightarrow OH + H$ | $k = 1.0 \times 10^{-10}$ |
| (R6)[a] | $H + O_2 \xrightarrow{+M} HO_2$ | $k_0 = 5.7 \times 10^{-32} (T/300)^{-1.6}$<br>$k_\infty = 7.5 \times 10^{-11}$ |
| (R7) | $CO + OH \rightarrow H + CO_2$ | $k = 1.5 \times 10^{-13} (1 + 0.6P)$ |
| (R8) | $HO_2 + NO \rightarrow NO_2 + OH$ | $k = 3.7 \times 10^{-12} \exp(240/T)$ |
| (R9) | $HO_2 + O_3 \rightarrow OH + 2O_2$ | $k = 1.1 \times 10^{-14} \exp(-500/T)$ |
| (R10) | $HO_2 + HO_2 \rightarrow H_2O_2 + O_2$ | $k = 2.3 \times 10^{-13} \exp(600/T)$ x $(1 + 1.4 \times 10^{-21} [H_2O] \exp(2200/T)$ |
| (R11) | $OH + H_2 \rightarrow H_2O + H$ | $k = 5.5 \times 10^{-12} \exp(-2000/T)$ |
| (R12) | $OH + O_3 \rightarrow HO_2 + O_2$ | $k = 1.6 \times 10^{-12} \exp(-940/T)$ |
| (R13)[a] | $OH + NO_2 \xrightarrow{+M} HNO_3$ | $k_0 = 2.6 \times 10^{-30} (T/300)^{-3.2}$<br>$k_\infty = 2.4 \times 10^{-11} (T/300)^{-1.3}$ |
| (R14)[a] | $OH + NO \xrightarrow{+M} HNO_2$ | $k_0 = 7.0 \times 10^{-31} (T/300)^{-2.6}$<br>$k_\infty = 1.5 \times 10^{-11} (T/300)^{-0.5}$ |
| (R15)[b] | $OH + HNO_3 \rightarrow H_2O + NO_3$ | $k_0 = 7.2 \times 10^{-15} \exp(785/T)^2$<br>$k_2 = 4.1 \times 10^{-16} \exp(1440/T)$<br>$k_3 = 1.9 \times 10^{-33} \exp(725/T)$ |
| (R16) | $OH + H_2O_2 \rightarrow H_2O + NO_3$ | $k = 2.9 \times 10^{-12} \exp(-160/T)$ |
| (R17) | $OH + HO_2NO_2 \rightarrow H_2O + O_2 + NO_2$ | $k = 1.3 \times 10^{-12} \exp(380/T)$ |
| (R18) | $OH + HO_2 \rightarrow H_2O + O_2$ | $k = 4.8 \times 10^{-12} \exp(250/T)$ |
| (R19) | $OH + HNO_2 \rightarrow H_2O + NO_2$ | $k = 6.6 \times 10^{-12}$ |
| (R20) | $HO_2NO_2 \xrightarrow{+M} HO_2 + NO_2$ | $k = k_{21}/(2.1 \times 10^{-27} \exp(10{,}900/T))$ |
| (R21)[a] | $HO_2 + NO_2 \xrightarrow{+M} HO_2NO_2$ | $k_0 = 1.8 \times 10^{-31} (T/300)^{-3.2}$<br>$k_\infty = 4.7 \times 10^{-12} (T/300)$ |
| (R22) | $C_2H_5 + O_2 \rightarrow C_2H_4 + HO_2$ | $k < 2.0 \times 10^{-15}$ |
| (R23) | $H_2O_2 \rightarrow$ deposition | $k = 2 \times 10^{-6}$-$1.07 \times 10^{-5}$ |
| (R24) | $HNO_3 \rightarrow$ deposition | $k = 2 \times 10^{-6}$-$1.07 \times 10^{-5}$ |
| (R25) | $HO_2NO_2 \rightarrow$ deposition | $k = 2 \times 10^{-6}$-$1.07 \times 10^{-5}$ |
| (R26) | $CH_3OOH \rightarrow$ deposition | $k = 2 \times 10^{-6}$-$1.07 \times 10^{-5}$ |
| (R27) | $OH + CH_4 \rightarrow CH_3 + H_2O$ | $k = 7.0 \times 10^{-15}$ |
| (R28)[a] | $CH_3 + O_2 \xrightarrow{+M} CH_3OO$ | $k_0 = 4.5 \times 10^{-31} (T/300)^{-3}$<br>$k_\infty = 1.8 \times 10^{-12} (T/300)^{-1.7}$ |
| (R29) | $O + CH_3 \rightarrow$ products | $k = 1.1 \times 10^{-10}$ |
| (R30) | $CH_3OO + HO_2 \rightarrow CH_3OOH + O_2$ | $k = 3.8 \times 10^{-13} \exp(780/T)$ |
| (R31) | $OH + CH_3OOH \rightarrow H_2O + CH_3OO$ | $k = 1.9 \times 10^{-12} \exp(190/T)$ |
| (R32) | $CH_3O + O_2 \rightarrow CH_2O + HO_2$ | $k = 3.9 \times 10^{-14} \exp(-900/T)$ |
| (R33) | $OH + CH_2O \rightarrow H_2O + HCO$ | $k = 1 \times 10^{-11}$ |
| (R34) | $HCO + O_2 \rightarrow CO + HO_2$ | $k = 0.7(3.5 \times 10^{-12} \exp(140/T))$ |
| (R35) | $CH_3OO + CH_3OO \rightarrow 2CH_3O + O_2$ | $k = 0.29(1.1 \times 10^{-13} \exp(365/T))$ |
| (R36) | $CH_3OO + NO \rightarrow CH_3O + NO_2$ | $k = 4.2 \times 10^{-12} \exp(180/T)$ |
| (R37) | $CH_2O \rightarrow$ deposition | $k = 2 \times 10^{-6}$-$1.07 \times 10^{-5}$ |
| (R38) | $NO + O_3 \rightarrow NO_2 + O_2$ | $k = 2.0 \times 10^{-12} \exp(-1400/T)$ |
| (R39) | $NO_3 + NO \rightarrow 2NO_2$ | $k = 1.7 \times 10^{-11} \exp(150/T)$ |
| (R40)[a] | $NO_3 + NO_2 \xrightarrow{+M} N_2O_5$ | $k_0 = 2.2 \times 10^{-30} (T/300)^{-4.3}$<br>$k_\infty = 1.5 \times 10^{-12} (T/300)^{-0.5}$ |

**Table 2.** (continued)

| | Reaction | Rate Coefficient |
|---|---|---|
| (R41) | $CH_2O + NO_3 \rightarrow HCO + HNO_3$ | $k = 5.8 \times 10^{-16}$ |
| (R42) | $SO_2 + HO_2 \rightarrow$ products | $k < 1.0 \times 10^{-18}$ |
| (R43)[a] | $N_2O_5 \xrightarrow{+N_2} NO_2 + NO_3$ | $k_0 = 2.2 \times 10^{-3} (T/300)^{-4.4} \exp(-11{,}080/T)$<br>$k_\infty = 9.7 \times 10^{14} (T/300)^{0.1} \exp(-11{,}080/T)$ |
| (R44) | $N_2O_5 + H_2O \rightarrow 2HNO_3$ | $k = 1.3 \times 10^{-21}$ |
| (R45) | $NO_2 + O_3 \rightarrow NO_3 + O_2$ | $k = 1.2 \times 10^{-13} \exp(-2450/T)$ |
| (R46) | $O + OH \rightarrow O_2 + H$ | $k = 2.2 \times 10^{-11} \exp(120/T)$ |
| (R47) | $O + HO_2 \rightarrow O_2 + OH$ | $k = 3.0 \times 10^{-11} \exp(200/T)$ |
| (R48) | $O + H_2O_2 \rightarrow O_2 + HO_2$ | $k = 1.4 \times 10^{-12} \exp(-2000/T)$ |
| (R49)[c] | $O + O_2 \xrightarrow{+M} O_3$ | $k_0 = (6.0 \times 10^{-34} (T/300)^{-2.3}) \times [M]$<br>$k_\infty = ..$ |
| (R50) | $OH + OH \rightarrow H_2O + O$ | $k = 4.2 \times 10^{-12} \exp(-240/T)$ |
| (R51)[a] | $OH + OH \xrightarrow{+M} H_2O_2$ | $k_0 = 6.9 \times 10^{-31} (T/300)^{-0.8}$<br>$k_\infty = 1.5 \times 10^{-11}$ |
| (R52) | $O_3$ + alkenes $\rightarrow$ products | $k = 1.2 \times 10^{-14} \exp(-2630/T)$ |
| (R53)[a] | $O + NO \xrightarrow{+M} NO_2$ | $k_0 = 9.0 \times 10^{-32} (T/300)^{-1.5}$<br>$k_\infty = 3.0 \times 10^{-11}$ |
| (R54)[a] | $O + NO_2 \xrightarrow{+M} NO_3$ | $k_0 = 9.0 \times 10^{-32} (T/300)^{-2.0}$<br>$k_\infty = 2.2 \times 10^{-11}$ |
| (R55) | $NO_3 + CO \rightarrow$ products | $k < 4.0 \times 10^{-19}$ |
| (R56) | $CH_3OOH + OH \rightarrow CH_2OOH + H_2O \rightarrow CH_2O + OH + H_2O$ | $k = 1.0 \times 10^{-12} \exp(190/T)$ |
| (R57) | $O + CH_2O \rightarrow OH + HCO$ | $k = 3.4 \times 10^{-11} \exp(-1600/T)$ |
| (R58) | $H_2S + NO_3 \rightarrow$ products | $k < 8.0 \times 10^{-16}$ |
| (R59) | $CH_2O + HO_2 \rightarrow$ adduct | $k = 6.7 \times 10^{-15} \exp(600/T)$ |
| (R60) | $O_3 + H \rightarrow OH + O_2$ | $k = 1.4 \times 10^{-10} \exp(-470/T)$ |
| (R61) | $H + HO_2 \rightarrow 2OH$ | $k = 0.9(8.1 \times 10^{-11})$ |
| (R62) | $O + HO_2NO_2 \rightarrow$ products | $k = 7.8 \times 10^{-11} \exp(-3400/T)$ |
| (R63) | $O(^1D) + CH_4 \rightarrow H_2 + CH_2O$ | $k = 1.4 \times 10^{-11}$ |
| (R64) | $O(^1D) + O_3 \rightarrow 2O_2$ | $k = 1.2 \times 10^{-10}$ |
| (R65) | $O(^1D) + O_3 \rightarrow O_2 + 2O$ | $k = 1.2 \times 10^{-10}$ |
| (R66) | $SO_2 + CH_3OO \rightarrow$ products | $k < 5.0 \times 10^{-17}$ |
| (R67) | $HO_2 + NO_3 \rightarrow OH + NO_2 + O_2$ | $k = 4.1 \times 10^{-12}$ |
| (R68) | $CH_3 + O_3 \rightarrow$ products | $k = 5..4 \times 10^{-12} \exp(-220/T)$ |
| (R69)[a] | $SO_2 + OH \rightarrow\rightarrow H_2SO_4$ | $k_0 = 3.0 \times 10^{-31} (T/300)^{-3.3}$<br>$k_\infty = 1.5 \times 10^{-12}$ |
| (R70) | $H_2S + OH \rightarrow\rightarrow SO_2$ | $k = 6.0 \times 10^{-12} \exp(-75/T)$ |
| (R71) | $SO_2 + O_3 \rightarrow$ products | $k = 3.0 \times 10^{-12} \exp(-7000/T)$ |
| (R72) | $SO_2 \rightarrow$ deposition | $k = (0.87 \times 10^{-2}$ m s$^{-1})$/(BLH) |
| (R73) | $NO_3 + OH \rightarrow HO_2 + NO_2$ | $k = 7.1 \times 10^{-11}$ |
| (R74) | $DMS_{(sw)} \rightarrow DMS_{(air)}$ | $k =$ DMS sea-to-air flux |
| (R75) | $H_2S_{(sw)} \rightarrow H_2S_{(air)}$ | $k = H_2S$ sea-to-air flux |
| (R76) | branching ratio for DMS oxidation (R89) | $k =$ branching ratio |
| (R77) | $O + O_3 \rightarrow 2O_2$ | $k = 8.0 \times 10^{-12} \exp(-2060/T)$ |
| (R78) | $O_3\ HNO_2 \rightarrow O_2 + HNO_3$ | $k < 5\ 0 \times 10^{-19}$ |
| (R79) | $CH_3OO + O_3 \rightarrow$ products | $k < 3.0 \times 10^{-17}$ |
| (R80) | $N_2O_5$ + aerosols $\rightarrow 2HNO_{3(aq)}$ | $k = 304$ |
| (R81) | $CH_3CO_3 + NO_2 \rightarrow$ PAN | $k = 4.7 \times 10^{-12}$ |
| (R82) | PAN $\rightarrow NO_2 + CH_3CO_3$ | $k = 1.9 \times 10^{16} \exp(-13{,}543/T)$ |
| (R83) | Alkenes + $NO_3 \rightarrow$ products | $k = 7.6 \times 10^{-15}$ |
| (R84) | $SO_2 + NO_2 \rightarrow$ products | $k < 2.0 \times 10^{-15}$ |
| (R85) | Alkanes + $NO_3 \rightarrow$ products | $k = 3.6 \times 10^{-17}$ |
| (R86) | $CH_3OO + CH_3OO \rightarrow CH_3OH + CH_2O + O_2$ | $k = 0.71(1.1 \times 10^{-13} \exp(365/T))$ |

**Table 2.** (continued)

| | Reaction | Rate Coefficient |
|---|---|---|
| (R87) | $NO_2 + NO_3 \rightarrow NO + NO_2 + O_2$ | $k = 8.2 \times 10^{-14} \exp(-1480/T)$ |
| (R88) | $NO_3 + DMS \rightarrow SO_2$ | $k = 1.1 \times 10^{-12}$ |
| (R89) | $OH + DMS \rightarrow$ products | $k = (T \exp(-234/T) + 8.4 \times 10^{-10} \exp(7230/T) + 2.68 \times 10^{-10} \exp(7810/T))/(1.04 \times 10^{11}\ T + 88.1 \exp(7460/T))$ |
| | $\rightarrow SO_2$ | $k = k_{76}\ k_{89}$ |
| | $\rightarrow$ MSA | $k = (1\text{-}k_{76})\ k_{89}$ |
| (R90)[a] | Alkenes + OH $\xrightarrow{+M}$ $HOCH_2CH_2$ | $k_0 = 1.5 \times 10^{-28} (T/300)^{-0.8}$<br>$k_\infty = 8.8 \times 10^{-12}$ |
| (R91)[c] | $O(^1D) + N_2 \xrightarrow{+M} N_2O$ | $k_0 = (3.5 \times 10^{-37} (T/300)^{-0.6}) \times [M]$<br>$k_\infty = ...$ |
| (R92) | $C_2H_5O_2 + C_2H_5O_2 \rightarrow$ products | $k = 1.6 \times 10^{-13} \exp(-300/T)$ |
| (R93) | $SO_2 + NO_3 \rightarrow$products | $k < 7.0 \times 10^{-21}$ |
| (R94) | $HO_2 + C_2H_5O_2 \rightarrow C_2H_5O_2H + O_2$ | $k = 6.5 \times 10^{-13} \exp(650/T)$ |
| (R95) | $OH$ + alkanes $\rightarrow C_2H_5$ | $k = 1.1 \times 10^{-11} \exp(-1100/T)$ |
| (R96)[a] | $C_2H_5 + O_2 \xrightarrow{+M} C_2H_5O_2$ | $k_0 = 2.0 \times 10^{-28} (T/300)^{-3.8}$<br>$k_\infty = 5.0 \times 10^{-12}$ |
| (R97) | $C_2H_5O_2 + NO \rightarrow C_2H_5O + NO_2$ | $k = 8.9 \times 10^{-12}$ |
| (R98) | $NO_3 + CH_3CHO \rightarrow HNO_3 + CH_3CO_3$ | $k = 1.4 \times 10^{-12} \exp(-1900/T)$ |
| (R99) | $O + CH_3CHO \rightarrow OH + CH_3O$ | $k = 1.8 \times 10^{-11} \exp(-1100/T)$ |
| (R100) | $CH_3CHO + OH \rightarrow CH_3CO_3 + H_2O$ | $k = 6.0 \times 10^{-12} \exp(250/T)$ |
| (R101) | $O + H_2S \rightarrow OH + SH$ | $k = 9.2 \times 10^{-12} \exp(250/T)$ |
| (R102) | $H + HO_2 \rightarrow H_2O + O$ | $k = 0\ 02(8.1 \times 10^{-11})$ |
| (R103) | $H + HO_2 \rightarrow H_2 + O_2$ | $k = 0.08(8.1 \times 10^{-11})$ |
| (R104) | $O + H_2 \rightarrow OH + H$ | $k = 4.11 \times 10^{-18}$ |
| (R105) | $CH_3CO_3 + NO \rightarrow CH_3 + CO_2 + NO_2$ | $k = 2.38 \times 10^{-12}$ |
| (R106) | $C_2H_5O_2H + OH \rightarrow C_2CH_2O_2H + H_2O$ | $k = 3.64 \times 10^{-12}$ |
| (R107) | $C_2H_5O_2H + OH \rightarrow C_2H_5O_2 + H_2O$ | $k = 5.95 \times 10^{-12}$ |
| (R108) | $O + NO_2 \rightarrow NO + O_2$ | $k = 6.5 \times 10^{-12} \exp(120/T)$ |
| (R109) | $O + NO_3 \rightarrow O_2 + NO_2$ | $k = 1.0 \times 10^{-11}$ |
| (R110) | $SO_2$ + aerosols $\rightarrow H_2SO_{4(aq)}$ | $k =$ user defined |
| (R111) | $O + HNO_3 \rightarrow OH + NO_3$ | $k = 3.0 \times 10^{-17}$ |
| (R112) | $HO_2 + HO_2 \xrightarrow{+M} H_2O_2 + O_2$ | $k = (1.7 \times 10^{-33} \exp(1000/T))$ [M] $(1 + 1.4 \times 10^{-21}[H_2O] \exp(2200/T)$ |
| (R113) | PAN $\rightarrow$ deposition | $k = 2 \times 10^{-6}$-$1.07 \times 10^{-5}$ |
| (R114) | $C_2H_5O + O_2 \rightarrow CH_3CO_3 + HO_2$ | $k = 1 \times 10^{-15}$ |
| (R115) | $C_2H_5O_2H \rightarrow$ deposition | $k = 2 \times 10^{-6}$-$1.07 \times 10^{-5}$ |
| (R116) | $CH_3CHO \rightarrow$ deposition | $k = 2 \times 10^{-6}$-$1.07 \times 10^{-5}$ |
| (R117) | $HO_2CH_3O_2 \rightarrow HO_2 + CH_3\ O_2$ | $k = 2.4 \times 10^{12} \exp(-7000/T)$ |
| (R118) | arbitrary NO source flux | $k =$ user defined |
| (R119) | $HO_2CH_3O_2 \rightarrow HO_2CH_3O_2H + O_2$<br>$HO_2CH_3O_2 \rightarrow HCO_2H + O_2 + H_2O$ | $k = 5.6 \times 10^{-15} \exp(230/T)$ |

**Table 2.** (continued)

| | Reaction | Rate Coefficient |
|---|---|---|
| (R120)[a] | $CH_3O_2 + NO_2 \xrightarrow{+M} CH_3O_2NO_2$ | $k_0 = 1.5 \times 10^{-30} (T/300)^{-4.0}$<br>$k_\infty = 6.5 \times 10^{-12} (T/300)^{-2.0}$ |
| (R121)[a] | $CH_3O_2NO_2 \xrightarrow{+N_2} CH_3O_2 NO_2$ | $k_0 = 9.5 \times 10^{-5} \exp(-9690/T)$<br>$k_\infty = 1.1 \times 10^{16} \exp(-10{,}560/T)$ |

[a] $k = \left(\frac{k_0[M]}{1+(k_0[M]/k_\infty)}\right) 0.6^{\left\{1+\left[\log_{10}(k_0[M]/k_\infty)\right]^2\right\}^{-1}}$

[b] $k = k_0 + \frac{k_3[M]}{1+(k_3[M]/k_2)}$

[c] $k = k_0[M]$ because $k_\infty$ is not available for this reaction.

All rate constants are from *NASA Evaluation 9* [1990] except: reactions (R72), (R81), (R82), (R83), and (R85), which are from *Russell et. al.* [1986], reaction (R89) which is from *Hynes et al.* [1986], reaction (R120) which is from *Johnston et al.* [1986], reactions (R104)-(R107), (R109)-(R111), and (R114) which are from *Thompson and Lenschow* [1984], and reactions (R27), (R30), (R31), (R35), (R43) (R56), (R86), (R117), (R119), and (R121) which are updated from *IUPAC Supplement IV* [1992]. Units for rate constants are as follows: unimolecular, $s^{-1}$ and bimolecular and pseudo bimolecular, $cm^3$ $molecule^{-1}$ $s^{-1}$.

the boundary layer height obtained from the radiosonde data, 2.2 km. An $O_3$ deposition velocity of 0.053 cm $s^{-1}$ is assumed from *Lenschow et al.* [1982]

The $NO_x$ concentration is estimated from previous measurements of NO made during SAGA 3 near 10°S, 145°W [*Torres and Thompson*, 1993], which had a mean value of 2.3 pmol $mol^{-1}$. $NO_x$ was calculated as 3 pmol $mol^{-1}$ from the photostationary state assumption, using the 24-hour mean photolysis rate for $NO_2$ and the observed mean $O_3$ concentration of 8 nmol $mol^{-1}$ [*Thompson et al.*, 1993]. Measurements of NO were also made during this study, however the data yielded only an upper limit of 15 pmol $mol^{-1}$ [D. Jaffe, personal communication, 1992]. In the model simulations discussed below, $NO_x$ is fixed throughout the model run but is distributed between the various reservoir species (NO, $NO_2$, $NO_3$, $N_2O_5$) kinetically.

**Table 3.** Photolysis Rate Coefficients Calculated in the Model

| | Reaction | Rate Coefficient |
|---|---|---|
| (RJ1) | $O_3 + h\nu \rightarrow O(^1D)$ | $J = jO_3$ |
| (RJ2) | $H_2O_2 + h\nu \rightarrow 2OH$ | $J = jH_2O_2$ |
| (RJ3) | $HNO_3 + h\nu \rightarrow OH + NO_2$ | $J = jHNO_3$ |
| (RJ4) | $HO_2NO_2 + h\nu \rightarrow OH + NO_3$ | $J = jHO_2NO_2$ |
| (RJ5) | $HNO_2 + h\nu \rightarrow OH + NO$ | $J = jHNO_2$ |
| (RJ6) | $CH_3OOH + h\nu \rightarrow CH_3O + OH$ | $J = jCH_3OOH$ |
| (RJ7) | $CH_2O + h\nu \rightarrow HCO + H$ | $J = jCH_2O_{(a)}$ |
| (RJ8) | $CH_2O + h\nu \rightarrow CO + H_2$ | $J = jCH_2O_{(b)}$ |
| (RJ9) | $NO_2 + h\nu \rightarrow NO + O$ | $J = jNO_2$ |
| (RJ10) | $NO_3 + h\nu \rightarrow NO_2 + O$ | $J = jNO_{3(a)}$ |
| (RJ11) | $N_2O_5 + h\nu \rightarrow NO_2 + NO_3$ | $J = jN_2O_5$ |
| (RJ12) | $C_2H_5O_2H + h\nu \rightarrow OH + C_2H_5O$ | $J = jC_2H_5O_2H$ |
| (RJ13) | $CH_3CHO + h\nu \rightarrow CH_3 + HCO$ | $J = jCH_3CHO$ |
| (RJ15) | $PAN (CH_3CO_4NO_2) + h\nu \rightarrow CH_3CO_3 + NO_2$ | $J = jPAN$ |
| (RJ16) | $NO_3 + h\nu \rightarrow NO + O_2$ | $J = jNO_{3(b)}$ |

from *Yvon and Saltzman*, [1993]

**Table 4.** Input Conditions for the Photochemical Model Calculations

| Parameter | Value | Source |
|---|---|---|
| $O_3$, nmol $mol^{-1}$ | 9.3 | J. Johnson (personal. Communication, 1992) |
| CO, nmol $mol^{-1}$ | 60.0 | J. Johnson (personal. Communication, 1992) |
| $CH_4$, μmol $mol^{-1}$ | 1.97 | *Bates et al.* [1993] |
| $H_2O_2$, pmol $mol^{-1}$ | 580 | *Thompson et al.* [1993] |
| $NO_x$, pmol $mol^{-1}$ | 3 | D. Jaffe (personal. Communication, 1992) |
| $C_2H_4$, pmol $mol^{-1}$ | 200 | *Donahue and Prinn* [1993] and *Atlas et al.*[1993] |
| $C_2H_6$, pmol $mol^{-1}$ | 800 | *Donahue and Prinn* [1993] and *Atlas et al.*[1993] |
| Temperature, K | 301.5 | J. Johnson (personal. Communication, 1992) |
| Total ozone column density, mmol $m^{-2}$ | 118 | P. Newman (personal. Communication, 1992) |
| Relative humidity, % | 72 | J. Johnson (personal. Communication, 1992) |
| DMS flux, μmol $m^{-2}$ $d^{-1}$ | 16 | *Yvon et al.* [this issue] |
| Boundary layer height, km | 2.2 | estimated from radiosondes |
| Vertical entrainment velocity, cm $s^{-1}$ | 0.168 | *Yvon et al.* [this issue] |
| $O_3$ deposition velocity, cm $s^{-1}$ | 0.053 | *Lenschow et al.* [1982] |

The total ozone column depth was obtained from the total ozone monitoring satellite (TOMS) (P. Newman, personal communication, 1992). The mean value for Julian days 63-71 at 12°S, 135°W was 118 mmol $m^{-2}$. As mentioned earlier, clear sky conditions are assumed for the determination of photolysis rate constants.

Vertical entrainment of air into the marine boundary layer from the free troposphere is included in these model calculations. The vertical entrainment velocity is estimated from a mass balance of ozone in the marine boundary layer at the MAGE station. Photochemical destruction and surface losses of ozone exceed the in situ photochemical source in the boundary layer in this region of the Pacific [*Johnson et al.*, 1990; *Thompson et al.*, 1993]. We assume that the additional ozone needed to maintain the observed mean concentration (9.3 nmol $mol^{-1}$) is provided via vertical entrainment and assume a free tropospheric $O_3$ concentration of 30 nmol $mol^{-1}$ [*Routhier et al.*, 1980; *Carroll et al.*, 1990]. Using this approach results in an entrainment velocity which is a function of the model mixing depth. The entrainment velocity is 0.25 cm $s^{-1}$ for a model mixing depth equal to the BLH of 2.2 km. This calculated entrainment velocity is in good agreement with those suggested by *Lenschow et al.* [1988], which range from 0.1 to 0.5 cm $s^{-1}$. For these model calculations the entrained air is assumed to contain no DMS [*Andreae et al.*, 1988, *Berresheim et al.*, 1990].

**Model simulations.** The photochemical model calculated a diel OH profile for the conditions observed at the MAGE station. The resulting midday maximum OH concentration for the MAGE station is 3 x $10^6$ molecules $cm^{-3}$, and the 24-hour mean OH concentration is 7 x $10^5$ molecules $cm^{-3}$ (Figure 5). This value is lower than the mean OH concentration of 9 x $10^5$ molecules $cm^{-3}$ calculated for SAGA 3 by *Thompson et al.* [1993] because the mean boundary layer ozone concentration measured during this cruise was at the low end of the ranges reported for SAGA 3.

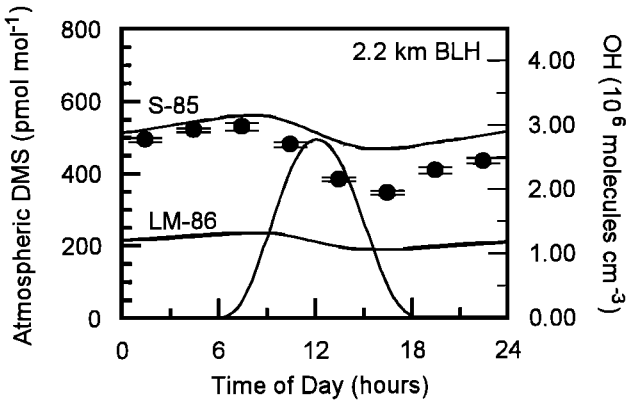


**Figure 5.** Results from model calculations using the S-85 and the LM-86 relationships between wind speed and gas exchange. The BLH is fixed at 2.2 km. The solid circles represent the averaged atmospheric DMS data from the MAGE station adjusted for solar noon as shown in Figure 4. The OH curve is plotted along the right-hand $y$ axis and has a noontime maximum.

The first two model runs examine the effect that the different fluxes (S-85 and LM-86) have on the calculated DMS concentrations (Figure 5). The LM-86 flux (9.7 μmol $m^{-2}$ $d^{-1}$) produces a mean atmospheric DMS mole fraction of 204 pmol $mol^{-1}$, which is only 45% of the observed concentration. The LM-86 relationship appears to substantially underestimate the gas transfer velocity. The S-85 flux (18.4 μmol $m^{-2}$ $d^{-1}$) yields a mean atmospheric DMS mole fraction of 515 pmol $mol^{-1}$ which is about 14% greater than the observed mole fraction. The flux needed to produce a mean DMS mole fraction of 450 pmol $mol^{-1}$ is 16.0 μmol $m^{-2}$ $d^{-1}$ (Figure 6).

The diel profiles shown in Figure 6 illustrate that the model significantly underestimates the observed amplitude in the diel cycle in atmospheric DMS concentrations. This result implies that the photochemical oxidation rate of DMS is underestimated by the model. In order to carry out a simulation which achieves both the mean concentration and the observed amplitude we must increase the oxidation rate above the rate currently accepted in photochemical models, and balance this increased loss by either (1) increasing the sea-to-air flux or (2) decreasing the mixing depth assumed for the model. We carried out several

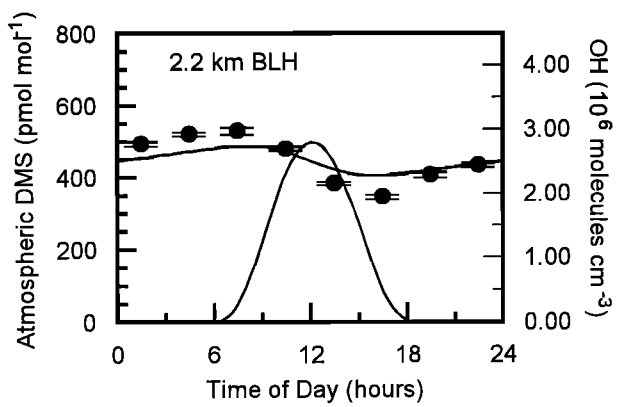


**Figure 6.** Results from model calculations assuming a 2.2 km BLH and a sea-to-air flux of 16.0 μmol $m^{-2}$ $d^{-1}$. The solid circles represent the averaged atmospheric DMS data from the MAGE station adjusted for solar noon as shown in Figure 4.

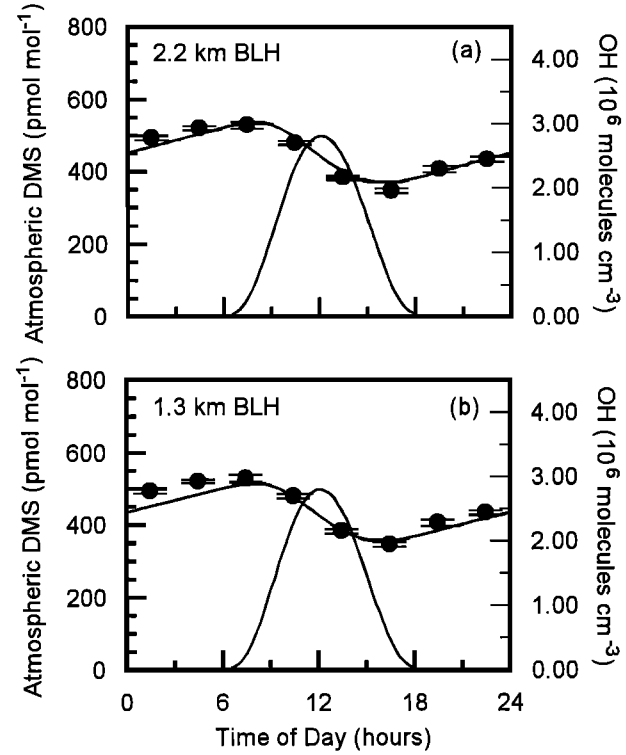


**Figure 7.** Results from model calculations attempting to reproduce the observed DMS diel cycle: (a) results from model calculations assuming a 2.2-km BLH, a sea-to-air flux of 28.0 μmol $m^{-2}$ $d^{-1}$, and a daytime oxidation rate twice that due to reaction with OH alone and (b) the results from a model run with the sea-to-air flux of DMS fixed at 16.0 μmol $m^{-2}$ $d^{-1}$, a BLH of 1.3 km, and a daytime oxidation rate twice that due to reaction with OH alone. The solid circles represent the averaged atmospheric DMS data from the MAGE station adjusted for solar noon as shown in Figure 4.

simulations to explore the sensitivity of the result to these parameters. In the first set of simulations we kept the model mixing depth fixed at 2.2 km, while increasing both the sea-to-air flux and the daytime oxidation rate of DMS. The daytime oxidation rate must be increased by 100% over that due to reaction with OH alone and the sea-to-air flux increased to 28.0 μmol $m^{-2}$ $d^{-1}$ to approach the observed diel cycle (Figure 7a).

In a second set of simulations we fixed the flux at 16.0 μmol $m^{-2}$ $d^{-1}$ while lowering the model mixing depth and increasing the daytime oxidation rate. A lower limit for the model mixing depth is the height of the mixed layer, which is 0.6 km for this station, as discussed earlier. An upper limit is the height at the top of the cloud-containing layer, which has a mean of 2.2 km for this station. Mixing between the mixed layer and the cloud-containing layer does occur, but it is slower than that within the mixed layer itself. If it is sufficiently slow, a gradient in DMS concentrations would exist between the top of the mixed layer and the trade wind inversion. This scenario can be simulated with the box model by assuming a model mixing depth between the two limits. The most reasonable solution is obtained by maximizing the model mixing depth and minimizing the increase in daytime oxidation rate necessary for the model to produce a DMS diel profile similar to that observed. In this case the best solution requires a model mixing depth of 1.3 km and a 100% increase in the daytime oxidation rate over that due to

reaction with OH alone to produce a diel cycle similar to that observed (Figure 7b).

The observed amplitude in the DMS diel cycle can be approached only if either the sea-to-air flux is increased or the model mixing depth is lowered, and the daytime oxidation rate must be doubled in both cases. We suggest two possible explanations: (1) there is a diel cycle in vertical entrainment with a midday or late afternoon maximum, or (2) the rate of the photochemical oxidation of DMS is underestimated by current photochemical models. A recent modeling study has shown that temporal variability in vertical mixing is more likely to dampen the DMS diel profile than to accentuate it [*Suhre and Rosset*, 1994]. There is some evidence from the diel profiles of $O_3$ (J. Johnson, personal communication) and $SO_2$ [*Yvon and Saltzman*, this issue] measured during this study that suggest a diel cycle in vertical entrainment with a nighttime maximum and a daytime minimum. Although there is no evidence from the radiosonde data to indicate the presence of a diel cycle in the vertical mixing, such a cycle could be used to explain the relatively constant levels of DMS observed between midnight and sunrise (Figure 4). However, this would also result in a dampening of the amplitude of the diel cycle in DMS. Thus the expected diel variation in vertical entrainment cannot explain the large amplitude of the DMS diel cycle.

The fact that the photochemical model cannot simulate the observed amplitude of the diel cycle without a large increase in the oxidation rate of DMS implies one or more of the following possibilities: (1) the DMS + OH rate constant is underestimated, (2) the model-generated OH concentrations are too low, or (3) additional photochemical oxidants are present in the marine boundary layer which are not accounted for in current photochemical models.

*Hynes* [1994] has noted that the rate constant for the reaction between DMS and OH may have been underestimated by up to 20%. There are two pathways for the oxidation of DMS by OH: (1) H atom abstraction and (2) OH addition In the OH addition pathway, OH reversibly forms an adduct with DMS. The short-lived adduct can decompose back to reactants or react with $O_2$. Therefore the effective rate coefficient is dependent on the partial pressure of $O_2$. It has been proposed that the products of the reaction between the adduct and $O_2$ include dimethylsulfone ($DMSO_2$) and OH [*Barnes et al.*, 1988; *Hynes*, 1994]. The techniques used to directly determined the reaction rate constant for DMS + OH involve monitoring the psuedo-first-order decay of OH in the presence of excess DMS. Any regeneration of OH during the experiment would cause a reduction in the rate of decay of OH, resulting in a lower estimate for the forward rate of DMS + OH adduct formation. This is not a limitation in studies where the rate constant is determined by using a competitive rate technique. *Barnes et al.* [1988] have determined a rate constant for DMS + OH of $8.0 \times 10^{-12}$ $cm^3$ $molecule^{-1}$ $s^{-1}$ at 298 K, using a competitive rate technique. This is 25% larger than the accepted value of $6\,3 \times 10^{-12}$ $cm^3$ $molecule^{-1}$ $s^{-1}$ at 298 K as determined from *Hynes et al.* [1986] on the basis of direct measurements. This discrepancy could be explained if OH regeneration were significant. However, if this hypothesis is true, the daytime oxidation rate would increase by only 25%, and we have shown in this study that the daytime oxidation rate must be increased by ~100% in order to account for the observed diel cycle

*Thompson and Stewart* [1991] assessed the uncertainty in model OH calculations, using a Monte Carlo technique. Those workers concluded that the quoted uncertainties in the rate constants used in photochemical calculations gives rise to an uncertainty of ±25% (1σ). This uncertainty alone is not sufficient to explain the discrepancy between the DMS oxidation rates generated by the model and those needed to simulate the DMS diel amplitude. Of course, clean marine air OH calculations remain essentially unverified by experimental measurements, and there may be additional sources of uncertainty in the reaction scheme which are not known.

*Keene et al.* [1990] suggested that reactive chlorine liberated from sea-salt aerosols may photolyze to generate Cl atoms in marine air. They suggested that if the process occurs, it could have a substantial impact on the oxidation rate of DMS in marine air, as the reaction between Cl and DMS is known to be extremely fast [*Stickel et al.*, 1992]. However, the evidence for the presence of Cl atoms in marine air is indirect, derived from estimates of chloride loss from aerosols and from mist chamber collection of an unknown gaseous chlorine-containing species in coastal air [*Pszenny et al.*, 1993]. If the precursor for Cl atoms is $Cl_2$, as suggested by *Keene et al.* [1990], the production of Cl atoms would have a significantly different diel profile from that of OH, with the maximum occurring just after sunrise. Therefore we would expect to see the daytime minimum shifted earlier in the day, rather than in the late afternoon as predicted from OH-only chemistry. The data do not preclude oxidation of DMS via chlorine atoms or other, as yet unidentified, oxidants. However, the observed DMS diel profile requires that any additional oxidants must have a diel profile similar to that of OH.

## Summary and Conclusions

Measurements of seawater and atmospheric DMS were made during an IGAC/MAGE cruise aboard the R/V *John V. Vickers* in the Tropical South Pacific Ocean in February and March of 1992. The data presented here were obtained at a station at 12°S, 135°W, which was occupied from March 3 to 10, 1992. In this study we presented measurements of the diel variability in DMS in the equatorial Pacific tropical trade wind regime and attempted to reconcile the measurements with photochemical model calculations.

The major conclusions of this study are as follows

1. The observed mean seawater concentration of 4.13 nM is higher than the 2.4 nM levels expected for tropical oligotrophic waters [*Andreae*, 1990]. The seawater DMS data exhibit a small diel cycle, while the atmospheric DMS data show a pronounced diel cycle with a mean mole fraction of 453 pmol $mol^{-1}$ and an amplitude of 85 pmol $mol^{-1}$.

2. The observed relationship between the mean oceanic and atmospheric DMS levels requires the use of an air-sea exchange coefficient which is at the upper limit end of the range of commonly used parameterizations. This study supports the gas transfer velocity versus wind speed parameterization based on $^{222}Rn$ deficit [*Smethie et al.*, 1985], but is not consistent with the *Liss and Merlivat* [1986] relationship or the dual tracer results of *Watson et al.* [1991]

3. The amplitude of the diel cycle in atmospheric DMS is significantly larger than that predicted by a photochemical model. The most straightforward way to reconcile the model with the observations is to (1) decrease the effective mixing height from the top of the cloud-containing layer (2.2 km) to an intermediate height (1 3 km) closer to the top of the mixed layer and (2) double the photochemical oxidation rate of DMS. This increase in the photochemical oxidation rate of DMS is greater than conventional estimates of the uncertainty in model estimates of OH and in the rate constant of the OH + DMS reaction It does not appear likely that dynamical effects such as

diel variations in the vertical entrainment rate can account for the large diel cycle of DMS.

**Acknowledgments.** We would like to thank Jim Johnson (NOAA/PMEL), Dan Jaffe (Univ. of Alaska), Paul Newman (NASA), Rick Artz (NOAA/ARL), and the Univ. of Miami's Remote Sensing Facility at RSMAS. This work was supported, in part, by a grant from the National Science Foundation (ATM-9120498), a NASA Climate and Global Change Fellowship (NGT-30114), and the Marine Sulfur, Aerosol and Climate component of the NOAA Climate and Global Change Program. Anne M. Thompson acknowledges support from an EOS Interdisciplinary Project (P. Brewer, PI).

## References

Andreae, M. O., Ocean-atmosphere interactions in the global biogeochemical sulfur cycle, *Mar. Chem., 30,* 1-29, 1990.

Andreae, M. O., and H. Raemdonck, Dimethyl sulfide in the surface ocean and the marine atmosphere: A global view, *Science, 221,* 744-747, 1983.

Andreae, M. O., R. J. Ferek, F. Bermond, K. P. Byrd, R. T. Engstrom, S Hardin, P. D. Houmere, F. LeMarrec, H. Raemdonck, and R. B. Chatfield, Dimethyl sulfide in the marine atmosphere, *J. Geophys. Res., 90,* 12891-12900, 1985.

Andreae, M. O., H. Berresheim, T. W. Andreae, M. A. Kritz, T. S Bates, and J T Merrill, Vertical distribution of dimethylsulfide, sulfur dioxide, aerosol ions, and radon over the northeast Pacific Ocean, *J. Atmos. Chem., 6,* 149-173, 1988.

Atlas, E., S. M. Schauffler, J T. Merill, C. J. Hahn, B. Ridley, J. Walega, J Greenberg, L. Heidt, and P. Zimmerman, Alkyl nitrates, nonmethane hydrocarbons, and halocarbon gases over the equatorial Pacific Ocean during SAGA 3, *J. Geophys. Res., 98,* 16,933-16,947, 1993.

Barnes, I., V. Bastian, and K. H. Becker, Kinetics and mechanisms of the reaction of OH radicals with dimethyl sulfide, *Int J. Chem. Kin., 20,* 415-431, 1988.

Bates, T. S., J D. Cline, R. H. Gammon, and S. R. Kelly-Hansen, Regional and seasonal variations in the flux of oceanic dimethylsulfide to the atmosphere. *J. Geophys. Res, 92,* 2930-2938, 1987.

Bates, T. S., J. E. Johnson, P. K Quinn, P. D. Goldan, W. C. Kuster, D. C. Covert and C. J. Hahn, The biogeochemical sulfur cycle in the marine boundary layer over the northeast Pacific Ocean, *J. Atmos Chem. 10,* 59-81, 1990.

Bates, T. S., B. K. Lamb, A. Guenther, J. Dignon, and R. E. Stoiber, Sulfur emissions to the atmosphere from natural sources, *J. Atmos Chem., 14,* 315-337, 1992.

Bates, T. S.., K. C. Kelly, and J. E. Johnson, Concentrations and fluxes of dissolved biogenic gases (DMS, $CH_4$, CO, $CO_2$) in the equatorial Pacific during the SAGA 3 experiment, *J Geophys. Res., 98,* 16,969-16,977, 1993.

Berresheim, H., M O. Andreae, G. P. Ayers, R. W. Gillett, J T. Merrill, V. J. Davis, and W. L. Chameides, Airborne measurements of dimethylsulfide, sulfur dioxide, and aerosol ions over the southern ocean south of Australia, *J. Atmos. Chem., 10,* 341-370, 1990.

Brimblecombe, P., and D. Shooter, Photo-oxidation of dimethylsulphide in aqueous solution, *Mar Chem., 19,* 343-353, 1986.

Carroll, M. A., *et al.*, Aircraft measurements of $NO_x$ over the Eastern Pacific and continental United States and implications for ozone production, *J. Geophys. Res., 95,* 10205-10234, 1990.

Charlson, R. J., J. E. Lovelock, M O. Andreae, and S. G. Warren, Oceanic phytoplankton, atmospheric sulfur, cloud albedo and climate, *Nature, 326,* 655, 1987.

Chatfield, R. B , and P. J. Crutzen, Sulfur dioxide in remote oceanic air· Cloud transport of reactive precursors, *J. Geophys. Res., 89,* 7111-7132, 1984

Cooper, D. J., and E. S. Saltzman, Measurements of atmospheric dimethylsulfide, hydrogen sulfide and carbon disulfide GTE/CITE 3, *J. Geophys. Res., 98,* 23,397-23,410, 1993.

Dacey, J. W. H., S. G. Wakeham, and B. L. Howes, Henry's law constants for dimethylsulfide in freshwater and seawater, *Geophys. Res. Lett., 11,* 991-994, 1984.

Donahue, N. M., and R. G. Prinn, In situ nonmethane hydrocarbon measurements on SAGA 3, *J. Geophys. Res., 98,* 16,915-16,933, 1993

Finlaysen-Pitts, B. J. and J N. Pitts Jr., *Atmospheric Chemistry: Fundamentals and Experimental Techniques,* John Wiley, New York, 1986.

Fraser, P. J., P. Hyson, R. A. Rasmussen, A. J. Crawford, and M. A. K. Khalil, Methane, carbon monoxide and methyl chloroform in the Southern Hemisphere, *J. Atmos. Chem., 4,* 3-42, 1986.

Graedel, T. E., Reduced sulfur emissions from the open oceans, *Geophys. Res. Lett., 6,* 329-331, 1979.

Griggs, M., Absorption coefficients of ozone in the ultraviolet and visible regions, *J. Chem. Phys., 49,* 857-859, 1968.

Holmen, K., and P. S. Liss, Models for air-water transfer: An experimental investigation, *Tellus, 36B,* 92-100, 1984.

Huebert, B. J., S. Howell, P. Laj, J. E. Johnson, P. K. Quinn, V. Yegorov, A. D. Clarke, and J. N. Porter. Observations of the atmospheric sulfur cycle on SAGA 3, *J. Geophys. Res., 98,* 16,985-16,995, 1993.

Hynes, A. J., Reaction mechanisms in atmospheric chemistry: Kinetic and studies of hydroxyl radical reactions, in *Spectroscopy in Environmental Science,* edited by R. J. H. Clark and R.E. Hester, John Wiley & Sons, Chichester, England, 1995.

Hynes, A. J., P. H Wine, and D. H. Semmes, Kinetics and mechanism of OH reactions with organic sulfides, *J. Phys. Chem., 90,* 4148-4156, 1986

IUPAC Subcommittee on Gas Kinetic Data Evaluation for Atmospheric Chemistry, R. Atkinson, D. L. Baulch, R. A. Cox, R. F. Hampson, J. A. Kerr, and J. Troe, Evaluated kinetic and photochemical data for atmospheric chemistry supplement IV *J. Phys. Chem. Ref. Data, 21,* 1125-1591, 1992.

Jähne, B., K. O. Münnich, R Bösinger, A. Dutzi, W. Heber, and P. Libner, On the parameters of air-water gas exchange, *J. Geophys. Res., 92,* 1937-1949, 1987.

Johnson, J. E., R. H. Gammon, J. Larsen, T. S. Bates, S. J. Oltmans, and J. C. Farmer, Ozone in the marine boundary layer over the Pacific and Indian Oceans: Latitudinal gradients and diurnal cycles, *J. Geophys. Res., 95,* 11847-11856, 1990.

Johnston, H. S., C. A. Cantrell, and J. G. Calvert, Unimolecular decomposition of $NO_3$ to form NO and $O_2$ and a review of $N_2O_5$ /$NO_3$ kinetics. *J. Geophys. Res., 91,* 5159-5172, 1986.

Keene, W. C , A. P. Pszenny, D. J. Jacob, R. A. Duce, J. N. Galloway, J. J. Schultz-Tokos, H. Sievering, and J. F. Boatman, The geochemical cycling of reactive chlorine through the marine troposphere, *Global Biogeochem Cycles, 4,* 407-430, 1990.

Kieber, D J., J. Jiao, R. P. Kiene and T. S. Bates, Impact of dimethylsulfide photochemistry on methyl sulfur cycling in the equatorial Pacific Ocean, *J Geophys. Res.*, in press

Kiene, R P , and T. S. Bates, Biological removal of dimethyl sulphide from seawater, *Nature, 345,* 702-705, 1990

Legrand, M. R., R. J. Delmas, and R. J. Charlson, Climatic forcing implications from Vostok ice-core sulphate data. *Nature, 334,* 418-420, 1988.

Legrand, M. R., C. Feniet-Saigne, E. S. Saltzman, C. Germain, N. I. Barkov, and V. N. Petrov, Ice-core record of oceanic emissions of dimethyl sulphide during the last climate cycle, *Nature, 350,* 144-146, 1991.

Lenschow, D H., R. Pearson Jr., and B. B. Stankov, Measurements of ozone vertical flux to ocean and forest, *J. Geophys. Res., 87,* 8833-8837, 1982.

Lenschow, D. H., I. R Paulch, A. R. Bandy, R. Pearson, Jr., S. R. Kawa, C. J. Weaver, B. J. Huebert, J. G. Kay, D. C. Thornton, and A. R. Driedger III, Dynamics and chemistry of marine stratocumulus (DYCOMS) experiment, *Bull. Am. Meteor. Soc., 69,* 1058-1067, 1988.

Liss, P. S., and L. Merlivat, Air-sea gas exchange rates: Introduction and synthesis, in *The Role of Air-Sea Exchange in Geochemical Cycling,* pp. 113-127, edited by P. Buat-Ménard, D. Reidel, Norwell, Mass., 1986.

Liss, P. S., and P. G. Slater, Flux of gases across the air-sea interface, *Nature, 247,* 181, 1974.

Logan, J. A., M. J. Prather, S. C. Wofsy, and M. B. McElroy, Tropospheric chemistry. a global perspective, *J. Geophys. Res., 86,* 7210-7254, 1981

Maroulis, P. J. and A. R. Bandy, Estimate of the contribution of biologically produced dimethyl sulfide to the global sulfur cycle, *Science, 196,* 647-648, 1977

Molina, L. T. and M. J. Molina, Absolute absorption cross sections of ozone in the 185 to 350-nm wavelength range, *J. Geophys. Res , 91,* 14,501-14,508, 1986.

NASA Panel for Data Evaluation, Chemical kinetics and photochemical data for use in stratospheric modeling. Evaluation number 9, edited by W. B. DeMore, D. M. Golden, R. F. Hampson, C. J. Howard, M. J. Kurylo, M J. Molina, A. R. Ravishankara, and S. P. Sander, *Publ. 87-41,* Jet Propul. Lab., Calif. Inst. of Technol., Pasadena, 1990.

Nguyen, B. C., B. Bonsang, and A. Gaudry, The role of the ocean in the global atmospheric sulfur cycle, *J. Geophys. Res.*, *88*, 10,903-10,914, 1983.

Press, W. H., B. P. Flannery, S. A. Teukolsky, and W. T. Vetterling, *Numerical Recipes: The Art of Scientific Computing*, Cambridge Univ. Press, New York, 1986.

Pszenny, A. A.P., W. C. Keene, D. J. Jacob, S. Fan, J. R. Maben, M. P. Zetwo, M. Springer-Young, and J. N. Galloway, Evidence of inorganic chlorine gases other than hydrogen chloride in marine surface air, *Geophys. Res. Lett.*, *20*, 699-702, 1993.

Quinn, P. K., T. S. Bates, J. E. Johnson, D. S. Covert, and R. J. Charlson, Interactions between the sulfur and reduced nitrogen cycles over the Central Pacific Ocean, *J. Geophys Res.*, *95*, 16405-16416, 1990

Routhier, F., R. Dennett, D. D. Davis, A. Wartburg, P. Haagenson, and A. C. Delany, Free tropospheric and boundary-layer airborne measurements of ozone over the latitude range of 58°S to 70°N, *J Geophys. Res.*, *85*, 7307-7321, 1980

Russell, A. G., G. R. Cass, and J. H. Seinfeld, On some aspects of nighttime atmospheric chemistry, *Environ. Sci. and Tech.*, *20*, 1167, 1986.

Saltzman, E. S., and D J Cooper, Shipboard measurements of atmospheric dimethylsulfide and hydrogen sulfide in the Caribbean and Gulf of Mexico, *J. Atmos. Sci.*, *7*, 191-209, 1988

Saltzman, E. S., D B. King, K. Holmen, and C. Leck, Experimental determination of the diffusion coefficient of dimethylsulfide in water, *J. Geophys. Res*, *98*, 16,481-16,486, 1993.

Shaw, G E., Bio-controlled thermostasis involving the sulfur cycle, *Climate Change*, *5*, 297-303, 1983.

Smethie, W. M., Jr, T. Takahashi, D W. Chipman, and J. R. Ledwell, Gas exchange and $CO_2$ flux in the tropical Atlantic Ocean determined from $^{222}Rn$ and $pCO_2$ measurements, *J Geophys. Res.*, *90*, 7005-7022, 1985.

Steele, L. P. E., E. J. Dlugokencky, P. M. Lang, P. P. Tans, R C Martin, and K A. Masarie, Slowing down of the global accumulation of atmospheric methane during the 1980s, *Nature*, *358*, 313-316, 1992.

Stickel, R. E., J. M. Nicovich, S. Wang, Z. Zhao, and P.H. Wine, Kinetic and mechanistic study of the reaction of atomic chlorine with dimethyl sulfide, *J. Phys. Chem*, *96*, 9875-9883, 1992.

Stull, R B., *An Introduction to Boundary Layer Meteorology*, Kluwer Acad., Norwell, Mass, 1988

Suhre, K., and R. Rosset, DMS oxidation and turbulent transport in the marine boundary layer: A numerical study, *J Atmos. Chem*, *18*, 379-395., 1994

Thompson, A. M., The effects of clouds on photolysis rates and ozone formation in the unpolluted troposphere, *J Geophys. Res.*, *89*, 1341-1349, 1984.

Thompson, A. M. and R. J. Cicerone, Clouds and wet removal as causes of variability in the trace-gas composition of the marine troposphere, *J. Geophys Res.*, *87*, 8811-8826, 1982.

Thompson, A. M. and D. H. Lenschow, Mean profiles of trace reactive species in the unpolluted marine surface layer, *J. Geophys Res.*, *89*, 4788-4796, 1984.

Thompson, A. M. and R. W. Stewart, Effect of kinetics uncertainties on calculated constituents in a tropospheric photochemical model, *J.Geophys. Res.*, *96*, 13089-13108, 1991.

Thompson, A. M., W. E. Esaias, and R. L. Iverson, Two approaches to determining the sea-to-air flux of dimethyl sulfide-satellite ocean color and a photochemical model with atmospheric measurements, *J. Geophys. Res.*, *95*, 551-558, 1990.

Thompson, A. M., *et al.*, Ozone observations and a model of marine boundary layer photochemistry during SAGA 3, *J. Geophys. Res.*, *98*, 16,955-16,968, 1993.

Toon, O. B., J. F. Kasting, R. P. Turco, and M. S. Liu, The sulfur cycle in the marine atmosphere, *J. Geophys. Res.*, *92*, 943-963, 1987.

Torres. A. L., and A. M. Thompson, Nitric oxide in the equatorial Pacific boundary layer: SAGA 3 measurements, *J. Geophys. Res.*, *98*, 16,949-16,954, 1993.

Upstill-Goddard, R. C., A. J. Watson, P. S. Liss, and M. I. Liddicoat, Gas transfer velocities in lakes measured with $SF_6$, *Tellus*, *42B*, 364-377, 1990.

Vaghjani, G. L., and A. R. Ravishankara, Absorption cross sections of $CH_3OOH$, $H_2O_2$, and $D_2O_2$ vapors between 210 and 365 nm at 297 K, *J. Geophys. Res.*, *94*, 3487-3492, 1989.

Watson, A. J., R. C. Upstill-Goddard, and P S. Liss, Air-sea gas exchange in rough and stormy seas measured by a dual-tracer technique, *Nature*, *349*, 145, 1991.

Wayne, R P, *et al*, The nitrate radical: Physics, chemistry, and the atmosphere, *Atmos. Environ.*, *25A*, 1-203, 1991.

Yvon, S. A., and E. S. Saltzman, A time-dependent photochemical box model for marine and atmospheric chemistry (PBMAC), *RSMAS Tech. Rep 93-008*, 78 pp., Univ. of Miami, Miami, Fla., 1993.

Yvon, S. A., and E. S. Saltzman, Atmospheric sulfur cycling in the tropical Pacific marine boundary layer (12°S, 135°W) A comparison of field data and model results, 2, Sulfur dioxide, *J. Geophys. Res.*, this issue

T S. Bates, NOAA Pacific Marine and Environmental Laboratory, 7600 Sand Point Way NE, Seattle, WA 98115. (bates@noaa.pmel.gov)

D J. Cooper, Plymouth Marine Laboratory, Prospect Place, Plymouth PL1 3DH, England. (dc@ibma.nerc-pml.ac.uk)

E S. Saltzman, Rosenstiel School of Marine and Atmospheric Science, University of Miami, 4600 Rickenbacker Cswy, Miami, FL 33149. (saltzman@rsmas miami.edu)

A M Thompson, NASA Goddard Space Flight Center, Greenbelt, MD 20771. (thompson@gator1 gsfc nasa.gov)

S. A. Yvon, NOAA Climate Monitoring and Diagnostics Laboratory, 325 Broadway, Boulder, CO 80303 (syvon@cmdl.noaa.gov)

(Received March 2, 1994; revised August 25, 1995;
accepted October 14, 1995.)